Indian Journal of Chemical Technology
Vol. 33, January 2026, pp. 80-93
DOI: 10.56042/ijct.v33i1.19162

Double diffusive bio-peristaltic propulsion of hydromagnetic Casson fluid through a conduit under the influence of Hall current and thermal radiation

Lipiya Vijayan & G. Sucharitha*

Department of Mathematics, School of Advanced Sciences, Vellore Institute of Technology, Vellore 632014, India
*E-mail: sucharitha.g@vit.ac.in

Received 26 April 2025; accepted 18 December 2025

Analysis of biological and industrial fluid pumping is an essential research domain due to its applications in various medical and industrial fields, including heart-related machinery, dialysis pumps, fluid-based drug delivery procedures, and industrial fluid transport techniques. As a result of this advancement, it is considered to describe the peristaltic transport of Casson nanofluid in a symmetric porous channel under double-diffusive magnetohydrodynamic (MHD) conditions. Also, consideration has been given to the impact of Hall current, inclined magnetic field, thermal radiation, and energy generation. To simplify the system, a lubrication approximation is used. The proposed dimensional governing principles are transformed into a system of dimensionless partial differential equations by incorporating suitable non dimensional components. The analytical solution for the temperature, concentration, and nanoparticle fraction is derived using the homotopy perturbation method (HPM). The exact solution of the stream function and velocity field is obtained. To further examine the properties of various parameters, including temperature, concentration, fluid velocity, pressure rise, nanoparticle volume fraction, and trapping phenomena, Nusselt and Sherwood numbers are thoroughly covered with graphical representations and tables. The analysis of the data demonstrates that in the presence of double-diffusive convection, the fluid's temperature can be raised by the Brownian motion parameter, the thermophoresis parameter, and the Dufour number. Additionally, the results are validated to verify excellent agreement between the present and past findings in a few specific circumstances.

Keywords: Casson fluid, Double diffusive convection, Hall current, Inclined magnetic field, Peristaltic transport, Porous medium, Symmetric channel, Thermal radiation

Introduction

Peristalsis is the movement of fluid along the length of the tube or channel wall as a gradual wave of contraction or expansion. The movement of the ovum in the female fallopian tube, the transport of spermatozoa, the chyme motion in the gastrointestinal tract, the movement of urine from the kidney to the bladder, and the swallowing of food through the oesophagus area few examples of the peristalsis mechanism. The practical and advantageous applications of peristalsis in bioengineering, medicine, and other fields have attracted the interest of many scholars and analysts. Initially, Latham[1] investigated the theoretical and scientific significance of peristaltic activity in several contexts. Furthermore, these findings concur with those of Fung & Yih[2] and Shapiro *et al.*[3]. Subsequently, this phenomenon has drawn the attention of several researchers, given advancements in various scientific and technological fields[4-10].

Materials with Newtonian fluidity, or viscosity that is constant at all applied shear rates, exhibit Newton's law of viscosity. Materials with flow properties that deviate from this behaviour are known as non-Newtonian fluids. Blood, paints, ketchup, honey, dyes, and pigments are a few instances of non-Newtonian fluids. As a result of the non-Newtonian fluid's medical and industrial uses, Nagarani and Sarojamma[11] studied the Casson fluid's peristaltic flow via an asymmetric two-dimensional conduit. After that, Nagarani[12] examined how an inclined channel affected Casson's peristaltic transport. In their application to the oesophageal flow of concentrated fluids, Pandey and Tripathi[13] investigated the peristaltic motion of Casson fluid in a finite conduit. Gudekote and Choudhari[14] examined the combined effects of slip and inclination on the peristaltic transit of Casson fluid in an elastic tube with porous walls. Due to their distinct rheological characteristics, non-Newtonian fluids play a vital role in both the industrial and medical sectors. These fluids may replicate the behaviour of biological fluids, such as blood and synovial fluid, which makes them essential for use in tissue engineering, drug delivery systems, and blood flow simulations in the medical industry.

This enables the simulation of physiological processes with greater precision and the delivery of therapeutic drugs with increased effectiveness. Non-Newtonian fluids are also utilized in implants and medical equipment to guarantee appropriate lubrication and reduce tissue injury. Several investigations have reported that peristaltic motion is impacted by non-Newtonian fluids.[15-17]

In the early twenty-first century, nanofluids gained popularity. Because of their substantial impact on the corresponding flow characteristics, these fluids keep attracting scientist's interest. This new class of nanotechnology-based heat-transfer fluids, known as "nanofluids" was initially coined by Choi[18]. They possess superior thermal properties compared to regular particle fluid suspensions or their host fluids. By uniformly dispersing and stabilising nanoparticle suspensions in host fluids, nanofluids aim to attain the best thermal characteristics at the lowest concentrations. Thermal control and effective, accurate fluid transfers are made possible by the coupling of peristalsis and nanofluids in various applications. The impact of wall characteristics on the peristaltic flow of nanofluid was examined by Mustafa *et al*.[19]. The transfer of copper-water nanofluid through peristaltic action in saturating porous media was investigated by Abbasi *et al*.[20]. The peristalsis of nanofluid in a non-uniform tube has been studied by Akbar *et al*.[21]. Diffusion effects on bi-viscous Bingham nanofluid mixed convective peristaltic flow through a porous medium with convective boundary conditions have been studied recently by Ajithkumar *et al*.[22]. Nadeem *et al*.[23] studied the movement of a porous peristaltic conduit carrying an Eyring-Powell nanofluid over a porous material.

The MHD effect of a conductive fluid can control fluid flow and optimize heat transfer. In other words, it regulates the fluid flow and maximizes heat transfer. Several researchers have expressed interest in studying MHD flows in various circumstances. Peristalsis with MHD is utilized in compressors to control normal blood circulation and in hyperthermia to regulate body temperature. Moreover, the effects of electrostatically conducting fluids in the presence of chemical reactions, heat radiation, and magnetic fields are relevant research subjects in many domains, including nuclear engineering, solar power technologies, and electric power generation. Because of this, Reddappa and Geetha[24] investigated the influence of a second-order chemical reaction on the MHD forced convection flow of Jeffrey nanofluid, which includes Cu, Ag, and Fe_3O_4 nanoparticles, over a moving plate situated in a porous medium with the effects of heat source and sink. Geetha *et al*.[25] analyzed the impact of double stratification on the MHD Williamson fluid flow and heat transfer over a shrinking/stretching sheet situated within a porous medium. Ajithkumar and Lakshminarayana[26] investigated chemically reactive Casson nanofluid MHD peristaltic flow in a non-uniform porous, inclined, and flexible conduit with a cross-diffusion effect. The studies pose a few pertinent questions regarding this topic[27,28].

The transfer of heat and mass within a hydraulic medium experiencing peristaltic motion is referred to as "heat and mass transfer" in peristalsis. The fluid is propelled forward during peristaltic transport through a sequence of contractions and expansions that occur along a tube or channel. Heat and mass transport events are caused by this motion's impact on the fluid's temperature and concentration distribution. Du four discovered through experimentation that the transfer of energy caused by a concentration gradient was what he named the thermal-diffusion effect. The diffusion-thermo effect (Soret), on the other hand, can also result in mass flux due to temperature gradients. It has numerous applications in industrial operations and biological systems. Magnetohydrodynamic wave propulsion of Bingham blood fluid with heat and mass transfer was studied by Eldabe *et al*.[29] across a non-uniform conduit. The consequences of an inclined magnetic field, heat, and mass peristalsis on blood in an inclined asymmetric channel were investigated by Abd-Alla *et al*.[30]. The chemically reactive Ellis fluid, investigated by Abbasi *et al*.[31] through peristaltic transport in an asymmetric conduit, was analysed with respect to heat and mass transfer. The transfer of heat and mass regarding peristaltic motion in MHD bioconvection of a Powell-Eyring fluid with changing thermal properties was investigated by Iqbal *et al*.[32]. The importance of heat and mass transmission in the peristaltic flow of Jeffrey material subjected to chemical and radiation processes through a non-uniform duct was investigated by Ravikumar *et al*.[33]. References[34-37] provide additional information about mass and heat transport in peristaltic flow.

A material with interconnected void spaces, or pores, that allow gases or liquids to move through is

referred to as a porous medium. Soil, rock, foam, and biological tissues are examples of these materials. To move materials through tubular structures, like the digestive tract, muscles must contract and relax rhythmically, a process known as peristalsis. This notion is used in porous media to characterize fluid flow that is caused by outside factors like pressure gradients or mechanical deformations of the porous material. This phenomenon is used in many domains, including soil mechanics, biotechnology, and medical engineering. Reddappa *et al*.[38] investigated the peristaltic motion of a conducting non-Newtonian Williamson fluid through a porous channel with flexible walls, considering the influence of thermal radiation. In an inclined passage, Gangavathi *et al*. [39] explored the impact of the slip boundary and Hall current effect on the peristaltic motion of a Jeffrey nanofluid through a porous medium. A couple of studies that have examined this area are listed in references[40,41].

Double diffusive convection is a phenomenon in fluid mechanics when convective currents are formed as a result of the concurrent diffusion of heat and mass. This occurs when temperature and concentration gradients in the fluid produce buoyancy-driven flow patterns. This has the potential to produce unique convective patterns and is essential for several natural and synthetic processes. Combined with peristalsis, double-diffusive convection can provide complex fluid dynamics situations. In the context of biomechanics and microfluidics, this intricate interaction influences phenomena such as liquid mixing in microchannels and nutrient absorption in the gastrointestinal tract. It is combined with double-diffusive convection, a process in which temperature and concentration gradients cause fluid motion. In recent years, researchers have also focused on the double-diffusive convection of peristalsis. When a thermally radiative Prandtl nanofluid flowed peristaltically in an irregular channel, Akram *et al*.[28] looked into the impact of an induced magnetic field on double diffusive convection. An asymmetric channel with partial slip and viscous dissipation effects was studied by Akram *et al*.[42] in the context of the convection theory of the thermally radiative peristaltic flow of Prandtl tilted magneto nanofluid. Fourth-grade nanofluid peristaltic flow in a uniform channel was investigated by Khan *et al*.[43] in relation to an inclined magnetic field and double-diffusion convection. In the context of heat radiation and a magnetic field, Ganesan and Vasanthakumari[44] investigated double-diffusive convection in peristaltic motion with Jeffrey nanofluids. Saeed *et al*.[45] looked at how an inclined magnetic field and partial slip-on double diffusion convection affected the peristaltic wave of a six-constant Jeffreys nanofluid along an asymmetric channel. The references[46-49] provide additional information about the double diffusion study.

Fortified by the success of the various investigations mentioned above, we examined how the heat source/sink, Hall current, and thermal radiation impact the Casson nanofluid double diffusion convective MHD peristaltic transport in a porous medium with an inclined magnetic field. Thermophoresis, Brownian motion, Soret and Dufour effects are all being investigated. To the best of our knowledge, no research has been done in the literature on the double diffusion convective peristaltic transport of Casson nanofluid under the mentioned physical conditions. An analytical solution is found for the resulting system of equations. A detailed discussion is provided, utilising graphical and tabular representations to illustrate the effects of several relevant parameters on velocity, temperature, concentration, nanoparticle volume fraction, Nusselt number, Sherwood number, and streamlines.

Mathematical Modelling

Consider the magnetohydrodynamic (MHD) peristaltic transport of an incompressible Casson nanofluid exhibiting double diffusive convection, together with the supplementary effects of thermal radiation. The flow is analysed within a symmetric, two-dimensional, porous channel with a width of $2d$. The channel walls demonstrate peristaltic motion, mimicking wave-like contractions and expansions that propel the fluid ahead. A Cartesian coordinate system is utilized to establish the geometry and flow characteristics. Within this framework, the X-axis aligns with the direction of wave propagation and extends along the channel's centreline, whereas the Y-axis is positioned perpendicular to the flow, including the channel's width. The fluid's velocity components are represented by U and V, corresponding to the X- and Y-directions, respectively. The peristaltic waves on the channel walls are assumed to propagate at a constant speed c in the positive X-direction. An inclined magnetic field of intensity B_0 has an impact on the suggested flow scenario.

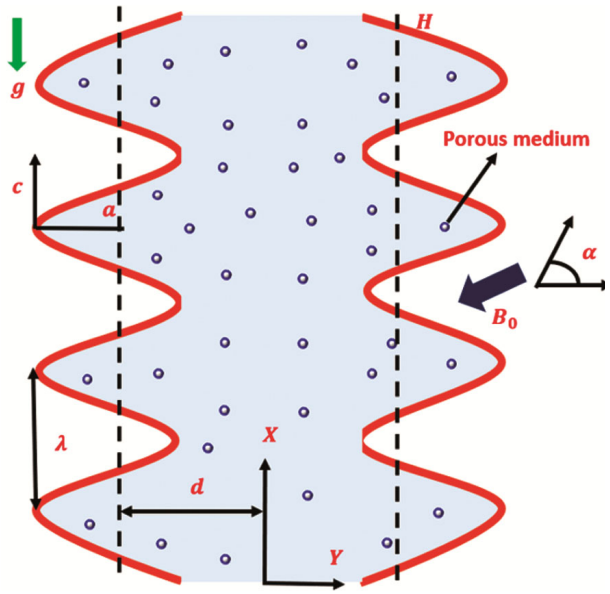

Fig. 1 — Flow geometry of the problem

Fig. 1 shows the schematic representation of the flow problem. $H(X,\bar{t})$ is the channel wall defined as the path taken by the sinusoidal wave with amplitude a, wavelength λ, and constant speed c.

$$H(X,\bar{t}) = d + asin\frac{2\pi}{\lambda}(X - c\bar{t}) \quad \ldots(1)$$

Here d represents thechannelhalf-width at the inlet and $\bar{t}$ denotes the time.

The double diffusive convective Casson fluid flows through a porous medium under the influence of mass transfer and heat when it is subject to the following basic governing equations[22,28,53]:

$$\frac{\partial U}{\partial X} + \frac{\partial V}{\partial Y} = 0 \quad \ldots(2)$$

$$\rho_f\left(\frac{\partial}{\partial \bar{t}} + U\frac{\partial}{\partial X} + V\frac{\partial}{\partial Y}\right)U = -\frac{\partial P}{\partial X} + \frac{\partial \tau_{XX}}{\partial X} + \frac{\partial \tau_{XY}}{\partial Y} - \frac{\sigma B_0^2}{(1+m^2)}(Ucos\alpha - Vsin\alpha)cos\alpha - \frac{\mu}{K}U + g\{(1-\Theta_0)\rho_{f_0}\{\beta_T(T-T_0) + \beta_C(C - C0 - \rho p - \rho f0\Theta - \Theta 0 \quad \ldots(3)$$

$$\rho_f\left(\frac{\partial}{\partial \bar{t}} + U\frac{\partial}{\partial X} + V\frac{\partial}{\partial Y}\right)V = -\frac{\partial P}{\partial Y} + \frac{\partial \tau_{YX}}{\partial X} + \frac{\partial \tau_{YY}}{\partial Y} + \frac{\sigma B_0^2}{(1+m^2)}(Ucos\alpha - Vsin\alpha)sin\alpha - \frac{\mu}{K}V \quad \ldots(4)$$

$$(\rho c)_f\left(\frac{\partial}{\partial \bar{t}} + U\frac{\partial}{\partial X} + V\frac{\partial}{\partial Y}\right)T = k\left(\frac{\partial^2 T}{\partial X^2} + \frac{\partial^2 T}{\partial Y^2}\right) + D_{TC}\left(\frac{\partial^2 C}{\partial X^2} + \frac{\partial^2 C}{\partial Y^2}\right) - \frac{\partial q_r}{\partial Y} + Q_0 + (\rho c)_p\left\{D_B\left(\frac{\partial \Theta}{\partial X}\frac{\partial T}{\partial X} + \frac{\partial \Theta}{\partial Y}\frac{\partial T}{\partial Y}\right) + \left(\frac{D_T}{T_0}\right)\left(\left(\frac{\partial T}{\partial X}\right)^2 + \left(\frac{\partial T}{\partial Y}\right)^2\right)\right\} \quad \ldots(5)$$

$$\left(\frac{\partial}{\partial \bar{t}} + U\frac{\partial}{\partial X} + V\frac{\partial}{\partial Y}\right)C = D_S\left(\frac{\partial^2 C}{\partial X^2} + \frac{\partial^2 C}{\partial Y^2}\right) + D_{CT}\left(\frac{\partial^2 T}{\partial X^2} + \frac{\partial^2 T}{\partial Y^2}\right) \quad \ldots(6)$$

$$\left(\frac{\partial}{\partial \bar{t}} + U\frac{\partial}{\partial X} + V\frac{\partial}{\partial Y}\right)\Theta = D_B\left(\frac{\partial^2 \Theta}{\partial X^2} + \frac{\partial^2 \Theta}{\partial Y^2}\right) + \left(\frac{D_T}{T_0}\right)\left(\frac{\partial^2 T}{\partial X^2} + \frac{\partial^2 T}{\partial Y^2}\right) \quad \ldots(7)$$

In the laboratory frame (X,Y), the motion appears unstable in its early stages; however, in the coordinate system (x,y), the motion is steady. When two reference frames are employed, the translation into Galilean is represented as follows:

$$\bar{u} = U - c\,,\bar{v} = V\,,\bar{x} = X - c\bar{t}\,,\bar{y} = Y\,,\bar{p}(x,y) = P(X,Y,\bar{t}) \quad \ldots(8)$$

The following parameters are used to generate the governing flow equations in dimensionless form:

$$\bar{x} = x\lambda\ ,\ \bar{y} = yd,\ \bar{u} = uc, \bar{v} = vc\ ,\ \bar{t} = \frac{t\lambda}{c}\ ,\ \delta = \frac{d}{\lambda}, \bar{p} = \frac{pc\mu\lambda}{d^2}, R_e = \frac{\rho_f cd}{\mu},$$

$$M = \sqrt{\frac{\sigma}{\mu}}B_0 d, G_r = \frac{g(1-\Theta_0)\rho_{f_0}\beta_T(T_1-T_0)d^2}{\mu c}, G_c = \frac{g(1-\Theta_0)\rho_{f_0}\beta_c(C_1-C_0)d^2}{\mu c},$$
$$G_f = \frac{g(\rho_p-\rho_{f_0})(\Theta_1-\Theta_0)d^2}{\mu c}, \theta = \frac{T-T_0}{T_1-T_0}, \phi = \frac{C-C_0}{C_1-C_0}, \chi = \frac{\Theta-\Theta_0}{\Theta_1-\Theta_0},$$
$$D_a = \frac{K}{d^2}\,, u = \frac{\partial \psi}{\partial y}, \quad \ldots(9)$$

$$v = -\delta\frac{\partial \psi}{\partial x}, P_r = \frac{(\rho c)_f\, v}{k}, N_b = \frac{\rho_p C_p D_B(\Theta_1 - \Theta_0)}{\mu C_f}, N_t = \frac{\rho_p C_p D_T(T_1 - T_0)}{T_0 \mu C_f}, N_{TC} = \frac{D_{TC}(C_1 - C_0)}{(T_1 - T_0)\mu C_f},$$
$$R_d = \frac{16\sigma^* T_0^3}{3k^*\mu C_f}, Q = \frac{Q_0 d^2}{(T_1-T_0)\mu C_f}, v = \frac{\mu}{\rho}, L_e = \frac{v}{D_s}, L_n = \frac{v}{D_B}, N_{CT} = \frac{D_{CT}(T_1-T_0)}{(C_1-C_0)D_s}.$$

Applying Eq. (9) under the presumption of a low Reynolds and long wavelength results in the following form for Eqs (3) – (7):

$$\frac{\partial p}{\partial x} = \left(1+\frac{1}{\beta}\right)\frac{\partial^3\psi}{\partial y^3} - \frac{M^2}{1+m^2}\left(\frac{\partial\psi}{\partial y}+1\right)(cos\alpha)^2 - \frac{1}{Da}\left(\frac{\partial\psi}{\partial y}+1\right) + G_r\theta + G_c\phi - G_f\chi \quad \ldots(10)$$

$$\frac{\partial p}{\partial y} = 0 \quad \ldots(11)$$

$$\frac{\partial^2\theta}{\partial y^2} + P_rN_b\left(\frac{\partial\chi}{\partial y}\frac{\partial\theta}{\partial y}\right) + P_rN_t\left(\frac{\partial\theta}{\partial y}\right)^2 + P_rN_{TC}\left(\frac{\partial^2\phi}{\partial y^2}\right) + P_rR_d\left(\frac{\partial^2\theta}{\partial y^2}\right) + P_rQ = 0 \quad \ldots(12)$$

$$\frac{\partial^2\phi}{\partial y^2} + N_{CT}\frac{\partial^2\theta}{\partial y^2} = 0 \quad \ldots(13)$$

$$\frac{\partial^2\chi}{\partial y^2} + \frac{N_t}{N_b}\frac{\partial^2\theta}{\partial y^2} = 0 \quad \ldots(14)$$

The subsequent statement outlines the non-dimensional representation of the boundary condition[28] necessary for resolving the PDE system (10) – (14).

$$\psi = 0, \frac{\partial^2\psi}{\partial y^2} = 0 \; at \; y = 0 \quad \ldots(15)$$

$$\psi = F, \frac{\partial\psi}{\partial y} = -1 \; at \; y = h \quad \ldots(16)$$

$$\theta = 0 \; at \; y = 0 \; and \; \theta = 1 \; at \; y = h \quad \ldots(17)$$

$$\phi = 0 \; at \; y = 0 \; and \; \phi = 1 \; at \; y = h \quad \ldots(18)$$

$$\chi = 0 \; at \; y = 0 \; and \; \chi = 1 \; at \; y = h \quad \ldots(19)$$

$$F = \int_0^h \frac{\partial\psi}{\partial y}\, dy, Q_* = F + 1 \quad \ldots(20)$$

Solution Methodology

HPM is an effective technique for resolving ordinary and partial nonlinear differential equations. Nonlinear differential equations, which can be challenging to solve using conventional analytical methods, describe a wide range of real-world phenomena. Using a homotopy operator, HPM converts these nonlinear equations into simpler auxillary equations, offering a methodical technique for solving them. With the use of this technique, we can generate analytical approximations to solutions that shed light on the system's behaviour. To acquire the analytical resolution of nonlinear partial differential Eqs (12) – (14), we can apply the homotopy perturbation method. According to the studies[50-52], we can write the equations as follows:

$$H(\theta,p) = (1-p)(L(\theta) - L(\theta_{10}) + p\left(L(\theta) + +B_1\left(\frac{\partial\chi}{\partial y}\frac{\partial\theta}{\partial y}\right) + B_2\left(\frac{\partial\theta}{\partial y}\right)^2 + B_3\left(\frac{\partial^2\phi}{\partial y^2}\right) + B_4\right) \quad \ldots(21)$$

$$H(\phi,p) = (1-p)(L(\phi) - L(\phi_{10}) + p\left(L(\phi) + C_1\frac{\partial^2\theta}{\partial y^2}\right) \quad \ldots(22)$$

$$H(\chi,p) = (1-p)(L(\chi) - L(\chi_{10}) + p\left(L(\chi) + D_1\frac{\partial^2\theta}{\partial y^2}\right) \quad \ldots(23)$$

where $L = \frac{\partial^2}{\partial y^2}$ is the linear operator and the initial assumptions θ_{10}, ϕ_{10} and χ_{10} can be stated as:

$$\theta_{10} = \frac{y}{h},\ \phi_{10} = \frac{y}{h},\ \chi_{10} = \frac{y}{h} \quad \ldots(24)$$

The key hypothesis to obtain the solution of the Eqs. (21) – (23) is given in the following power series in p.

$$\theta(y,p) = \theta_0 + \theta_1 p + \theta_2 p^2 + \theta_3 p^3 + \cdots \quad \ldots(25)$$

$$\phi(y,p) = \phi_0 + \phi_1 p + \phi_2 p^2 + \phi_3 p^3 + \cdots \quad \ldots(26)$$

$$\chi(y,p) = \chi_0 + \chi_1 p + \chi_2 p^2 + \chi_3 p^3 + \cdots \quad \ldots(27)$$

Following the substitution of Eqs (25) – (27) into (21) – (23), the system of partial differential equations and the suitable boundary condition are obtained. Only the zeroth, first, second, and third order systems of PDEs were investigated for the convergence of solutions, since highorder systems are negligible for the tiny homotopy perturbation parameter p.

The following is a description of the analytical solutions for temperature, concentration, and nanoparticle volume fraction (for $p = 1$).

(a) Zeroth–order system

$$\frac{\partial^2\theta_0}{\partial y^2} = 0 \quad \ldots(28)$$

$$\frac{\partial^2\phi_0}{\partial y^2} = 0 \quad \ldots(29)$$

$$\frac{\partial^2\chi_0}{\partial y^2} = 0 \quad \ldots(30)$$

$$\theta_0 = 0 \text{ at } y = 0, \theta_0 = 1 \text{ at } y = h$$
$$\phi_0 = 0 \text{ at } y = 0, \phi_0 = 1 \text{ at } y = h$$
$$\chi_0 = 0 \text{ at } y = 0, \chi_0 = 1 \text{ at } y = h \quad \ldots(31)$$

(b) First – order system

$$\frac{\partial^2\theta_1}{\partial y^2} + B_1\left(\frac{\partial\chi_0}{\partial y}\frac{\partial\theta_0}{\partial y}\right) + B_2\left(\frac{\partial\theta_0}{\partial y}\frac{\partial\theta_0}{\partial y}\right) + B_3\left(\frac{\partial^2\phi_0}{\partial y^2}\right) + B_4 = 0 \quad \ldots(32)$$

$$\frac{\partial^2\phi_1}{\partial y^2} + C_1\frac{\partial^2\theta_0}{\partial y^2} = 0 \quad \ldots(33)$$

$$\frac{\partial^2\chi_1}{\partial y^2} + D_1\frac{\partial^2\theta_0}{\partial y^2} = 0 \quad \ldots(34)$$

$$\theta_1 = 0 \text{ at } y = 0, \theta_1 = 0 \text{ at } y = h$$
$$\phi_1 = 0 \text{ at } y = 0, \phi_1 = 0 \text{ at } y = h$$
$$\chi_1 = 0 \text{ at } y = 0, \chi_1 = 0 \text{ at } y = h \quad \ldots(35)$$

(c) Second–order system

$$\frac{\partial^2\theta_2}{\partial y^2} + B_1\left(\frac{\partial\chi_0}{\partial y}\frac{\partial\theta_1}{\partial y} + \frac{\partial\chi_1}{\partial y}\frac{\partial\theta_0}{\partial y}\right) + B_2\left(\frac{\partial\theta_0}{\partial y}\frac{\partial\theta_1}{\partial y} + \partial\theta 1\partial y\partial\theta 0\partial y + B3\partial 2\phi 1\partial y2 = 0\right) \quad \ldots(36)$$

$$\frac{\partial^2\phi_2}{\partial y^2} + C_1\frac{\partial^2\theta_1}{\partial y^2} = 0 \quad \ldots(37)$$

$$\frac{\partial^2\chi_2}{\partial y^2} + D_1\frac{\partial^2\theta_1}{\partial y^2} = 0 \quad \ldots(38)$$

$$\theta_2 = 0 \text{ at } y = 0, \theta_2 = 0 \text{ at } y = h$$
$$\phi_2 = 0 \text{ at } y = 0, \phi_2 = 0 \text{ at } y = h$$
$$\chi_2 = 0 \text{ at } y = 0, \chi_2 = 0 \text{ at } y = h \quad \ldots(39)$$

(d) Third–order system

$$\frac{\partial^2\theta_3}{\partial y^2} + B_1\left(\frac{\partial\chi_0}{\partial y}\frac{\partial\theta_2}{\partial y} + \frac{\partial\chi_1}{\partial y}\frac{\partial\theta_1}{\partial y} + \frac{\partial\chi_2}{\partial y}\frac{\partial\theta_0}{\partial y}\right) + B_2\left(\frac{\partial\theta_0}{\partial y}\frac{\partial\theta_2}{\partial y} + \frac{\partial\theta_1}{\partial y}\frac{\partial\theta_1}{\partial y} + \partial\theta 2\partial y\partial\theta 0\partial y + B3\partial 2\phi 2\partial y2 = 0\right) \quad \ldots(40)$$

$$\frac{\partial^2\phi_3}{\partial y^2} + C_1\frac{\partial^2\theta_2}{\partial y^2} = 0 \quad \ldots(41)$$

$$\frac{\partial^2\chi_3}{\partial y^2} + D_1\frac{\partial^2\theta_2}{\partial y^2} = 0 \quad \ldots(42)$$

$$\theta_3 = 0 \text{ at } y = 0, \theta_3 = 0 \text{ at } y = h$$
$$\phi_3 = 0 \text{ at } y = 0, \phi_3 = 0 \text{ at } y = h$$
$$\chi_3 = 0 \text{ at } y = 0, \chi_3 = 0 \text{ at } y = h \quad \ldots(43)$$

Hence, the following is a description of the analytical expressions for the temperature, concentration, and nanoparticle fraction (for $p = 1$):

$$\theta = T_{21}y^4 + T_{24}y^3 + T_{25}y^2 + T_{26}y + T_{27} \quad \ldots(44)$$

$$\phi = E_{14}y^3 + E_{16}y^2 + E_{17}y + E_{18} \quad \ldots(45)$$

$$\chi = N_{14}y^3 + N_{16}y^2 + N_{17}y + N_{18} \quad \ldots(46)$$

We can find an exact solution for velocity by using (11) and incorporating (44) - (46) into Eq. (10):

$$u = A_2 + 2A_3y + 3A_4y^2 + 4A_5y^3 + 5A_6y^4 + NA_7\cosh Ny + NA_8\sinh Ny \quad \ldots(47)$$

We used boundary conditions (15) to (19) to calculate all arbitrary constants. The computed values for these constants are shown in the Appendix.

The following are the expressions for the Nusselt and Sherwood numbers at the wall[50]:

$$Nus = -(1 + R_dP_r)\left(\frac{\partial\theta}{\partial y}\right)_{at\ y=h} \quad \ldots(48)$$

$$Shr = -\left(\frac{\partial\phi}{\partial y}\right)_{at\ y=h} \quad \ldots(49)$$

Results and Discussion

The primary purpose of this section is to investigate the impact of controlling factors on the flow paradigm. A detailed discussion is held regarding the graphical behaviour of temperature, velocity, concentration, nanoparticle volume fraction, pressure rise and streamlines. The impact of numerous pertinent flow factors on the fluid flow is analysed using MATLAB software. Additionally, the characteristics of both Sherwood and Nusselt numbers are examined through the creation of tables. Since this channel is symmetric, we only considered half of it when plotting.

Temperature profile

Figs $2(a) - 2(e)$ demonstrate the variance in temperature distribution for different values of the following parameters such asN_b, N_t, N_{TC}, Q, and R_d.The temperature profile rises as a result of the increased values of parameters N_b, N_t, N_{TC}, and Q. Figs $2(a)$ and 2(b) show the combined analysis of the thermophoresis and Brownian parameters in θ. With rising values of N_b and N_t, these figures show that the temperature rises. The rise in Brownian motion intensity speeds up the flow of the nanoparticles along the fluid wall, which raises the temperature along with N_b and N_t. Fig. 2(c) illustrates that thermal diffusion has a greater effect when the Dufour number is high, although both mass and heat flow contribute to the temperature of the fluid profile. Fig. $2(d)$ shows the connection between the temperature profile and the heat source/sink parameter Q. Temperature rises are caused by an increase in the specific heat of the nanofluid as Q value rises. In accordance with Fig. 2(e), a decrease in θ is caused by an increase in R_d. Radiation effect suppresses the temperature profile and slows down the rate of energy transfer to the fluid.

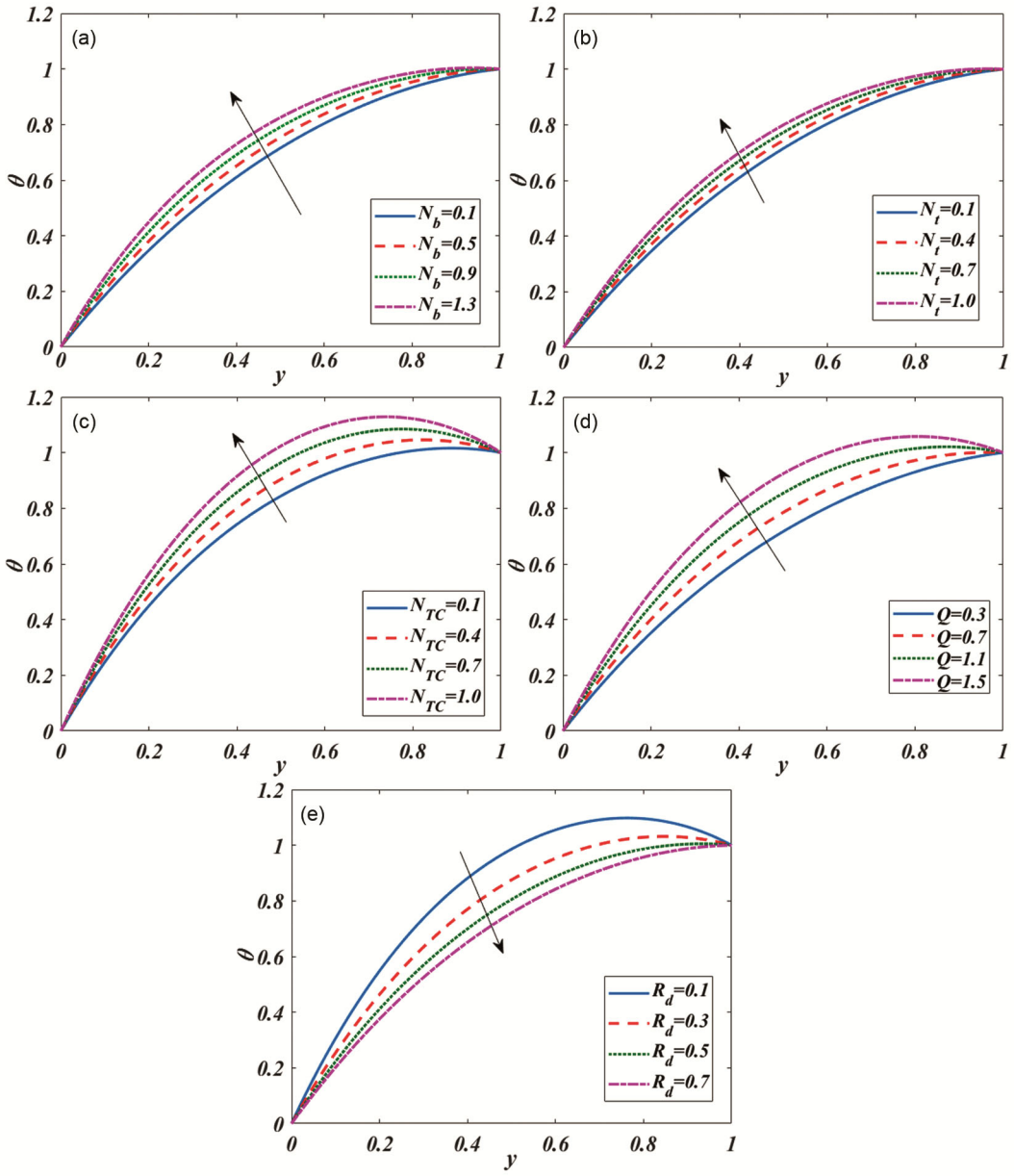

Fig. 2 — The temperature profiles (θ) with variations in (a) N_b, (b) N_t, (c) N_{TC}, (d) Q and (e) R_d

Concentration profile

The impacts of several parameters on the concentration distribution are displayed in Figs $3(a)-3(d)$. Fig. $3(a)$ shows how the concentration affects the behaviour of the Brownian motion parameter. It has been seen that the concentration distribution shrinks as N_b values rise. Nanoscale particles randomly moving from channel walls to substances is the cause of it. It also happens because any increase in Brownian motion accelerates the random motion that disperses the nanoparticles and, as a result, reduces concentration. The outcome of N_t and N_{CT} on ϕ are depicted in Figs $3(b)$ and $3(c)$. For the thermophoresis parameter N_t and Soret number N_{CT} similar findings have been noted. The concentration profile is diminished by boosting N_t and N_{CT} values. This occurs as a result of a substantial nanoparticle transit from a heated to a cooled area. Fig. $3(d)$ explores the fluctuation of the heat radiation concentration profile. It has been demonstrated that concentration increases as a result of increasing thermal radiation impacts. The existence of thermal radiation can lead to a variable distribution of fluid temperature and concentration.

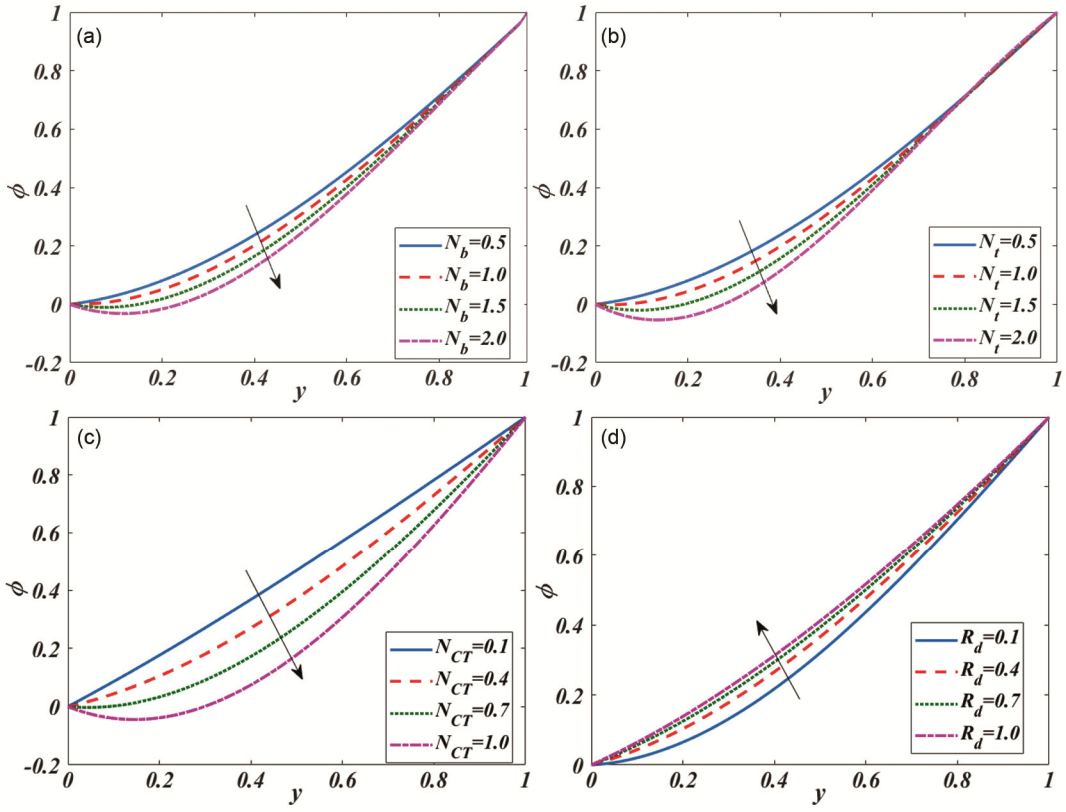

Fig. 3 — The concentration profiles (ϕ) with variations in (a) N_b, (b) N_t, (c) N_{CT}, and (d) R_d

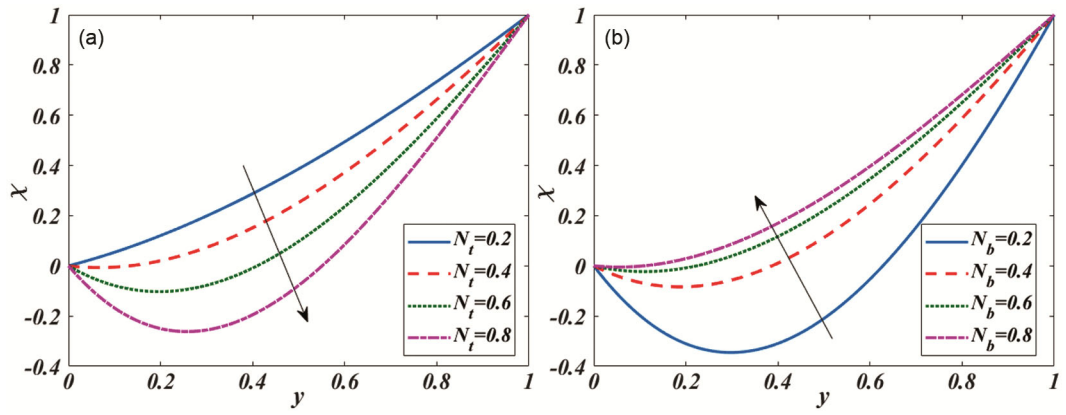

Fig. 4 — The nanoparticle fraction profiles (χ) with variations in (a) N_t and (b) N_b

Nanoparticle volume fraction profile

Figs $4(a) - 4(b)$ display the plots that highlight the impact of N_t and N_b on the fraction of nanoparticles. According to these plots, as thermophoresis values increase, the proportion of nanoparticles declines; however, an opposite trend is observed for the Brownian motion values. This can be attributed to the inverse connection between N_t and $N_b$with nanoparticle fraction.

Velocity Profile

The velocity profile is affected by several physical characteristics, as seen in Figs $5(a) - 5(h)$. To describe the momentum and heat transmission mechanisms through internal flows, the fluid velocity is a crucial factor. Fig. $5(a)$ is plotted for analysing the effects of Casson fluid parameter β. In the middle of the channel, it is evident that the velocity profile decelerates, and it rises near the wall. This behaviour

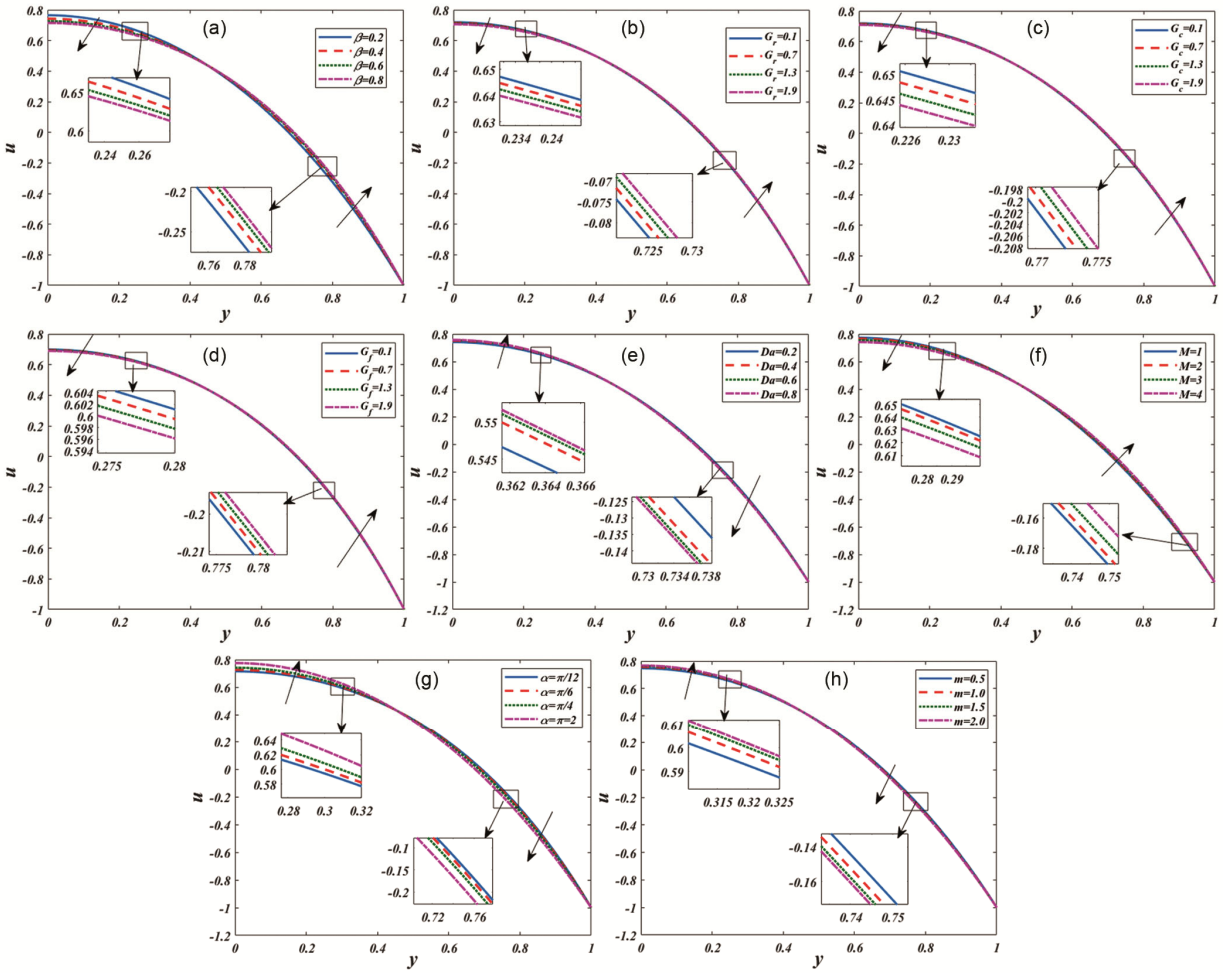

Fig. 5 — The velocity profiles (u) with variations in (a) β, (b) G_r, (c) G_c, (d) G_f, (e) Da, (f) M, (g) α and (h) m

results from the variations in the fluid viscosity, which lowers the yield stress when the Casson parameter values are increased. Figs $5(b) - 5(d)$ represents the effect of thermal Grashof number G_r, solutal Grash of number G_c, and nanoparticle Grashof number G_f, on fluid velocity. Franz Grashof invented the Grashof parameter, which bears his name, in 1896. When examining free or natural convection, this dimensionless variable is essential. The Grashof number is the ratio of buoyant force to viscous hydrodynamic force. As we have seen, the velocity of the fluid declines in the centre of the channel and increases close to the wall in the pictures when G_r, G_c, and G_f increases. The effect of the Darcy parameter Da on the fluid velocity was investigated in Fig. 5(e). This picture demonstrates that there is a rise in the fluid velocity in the centre of the channel, while it declines at the right wall of the channel. The reason for this could be that porous material separates the fluid particles. The influence of the magnetic parameter M on the velocity distribution is discussed in Fig. 5(f). The fluid velocity increases close to the right wall and decreases in the middle of the channel for higher values of M. This is because, in an electrically conductive fluid, an increase in the applied magnetic field tends to increase the opposite force, also known as the Lorentz force, which causes the fluid velocity to drop in the centre region of the fluid. Fig. 5(g) demonstrates that, in the centre region, the velocity field increases with α (angle of magnetic field), whereas near the right end of the wall, it decreases. For different values of the Hall parameter m, the fluid velocity result is shown in Fig 5(h). It demonstrates that when m rises, velocity increases in the middle of the channel. The Hall effect provides a modest physical balance to the magnetic component of the applied magnetic field.

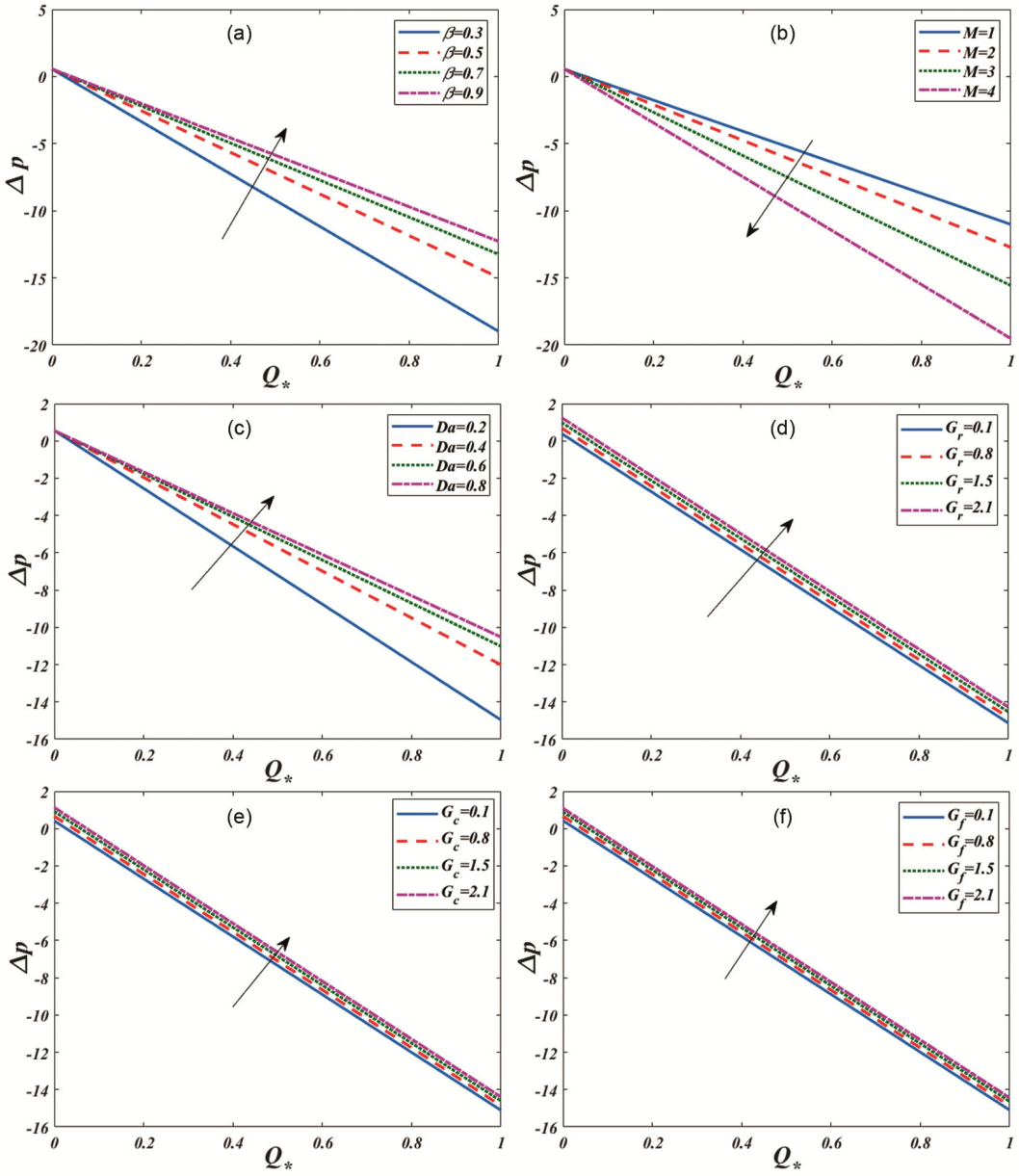

Fig. 6 — The pressure rise profiles (Δp) with variations in (a) β (b) M, (c) Da, (d) G_r, (e) G_c and (f) G_f

Pressure rise

Figs $6(a) - 6(f)$ demonstrate the pressure rises on some parameters. The following groupings of pumping zones are used to study the characteristics of pressure rise: (i) the part of the peristaltic ($Q_* > 0, \Delta p > 0$) when fluid is moved along its propagation track and pressure is regulated by peristalsis waves. (ii) the augmented zone ($Q_* > 0, \Delta p < 0$) peristalsis-induced pressure in this area boosts flow. (iii) the retrograde zone ($Q_* < 0, \Delta p > 0$) where the flow is being resisted by peristalsis, and (iv) the only source of flow in the free pumping area ($\Delta p = 0$) is the peristalsis wall. The augmented zone experiences an increase in pressure due to the fluid parameter's rise, as illustrated in Fig. $6(a)$. Whereas Fig. $6(b)$ illustrates an increase in the magnetic parameter causes a decline in pressure rise. In accordance with Fig. 6(c), pressure rise accelerates as the Darcy parameter values climb. At higher G_r, G_c, and G_f values, we see pressure increases in all peristaltic zones, as shown in Figs $6(d)$ -$6(f)$.

A critical aspect of peristaltic transport is the phenomenon of trapping. It begins with the internal movement of a fluid mass surrounded by streamlines

from peristaltic waves. Figs 7, 8, 9 examine streamline deviations for various values of pertinent parameters. These graphs show that an increase in the parameters M, R_d, and Da causes the bolus size to rise.

Table I displays the variation in Sherwood and Nusselt numbers for various relevant factor values. As the values of the Brownian motion, thermophoresis, Dufour, heat source/sink, and Soret parameters

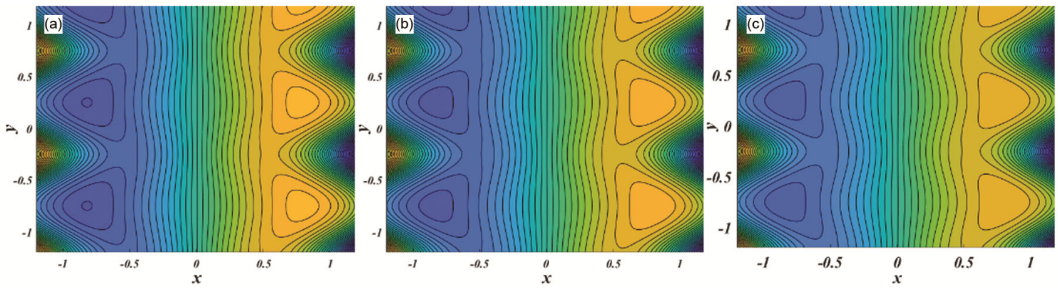

Fig. 7 — Streamlines behaviour on $M = (a)1, (b)\ 2\ and\ (c)3$

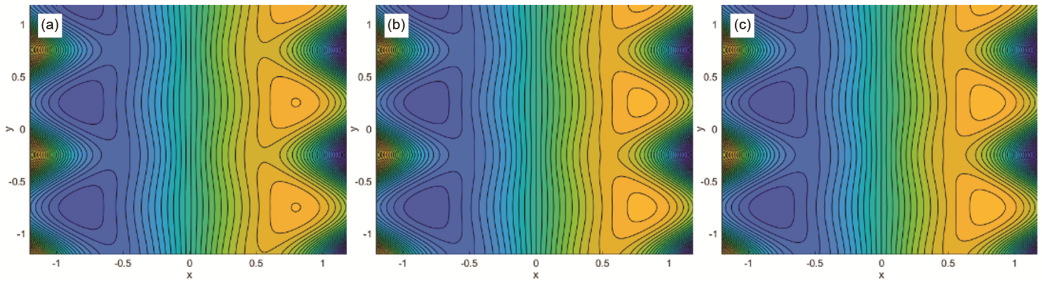

Fig. 8 — Streamlines behaviour on $R_d = (a)0, (b)\ 1\ and\ (c)2$

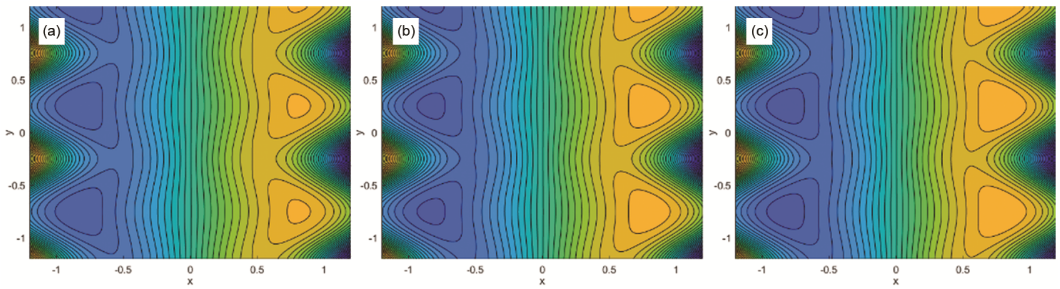

Fig. 9 — Streamline behaviour on $Da = (a)0.2, (b)0.3\ and\ (c)0.4$

Table 1 — Variations inSherwood andNusselt numbers for values of relevant parameters

P_r	N_b	N_t	R_d	Q	N_{CT}	*Nus*	*Shr*
0.2						-0.9030	-1.1144
0.4						-0.6091	-1.2100
0.6						-0.3150	-1.2900
	0.1					-0.5649	-1.2188
	0.3					-0.5128	-1.2356
	0.5					-0.4622	-1.2518
		0.1				-0.5731	-1.2260
		0.3				-0.5178	-1.2396
		0.5				-0.4622	-1.2518
			0.1			-0.3882	-1.2622
			0.2			-0.4622	-1.2518
			0.3			-0.5386	-1.2422
				0.2		-0.8495	-1.1209
				0.4		-0.7904	-1.1410
				0.6		-0.7312	-1.1612
					0.2	-0.5242	-1.0645
					0.4	-0.4932	-1.1289
					0.6	-0.4622	-1.1934

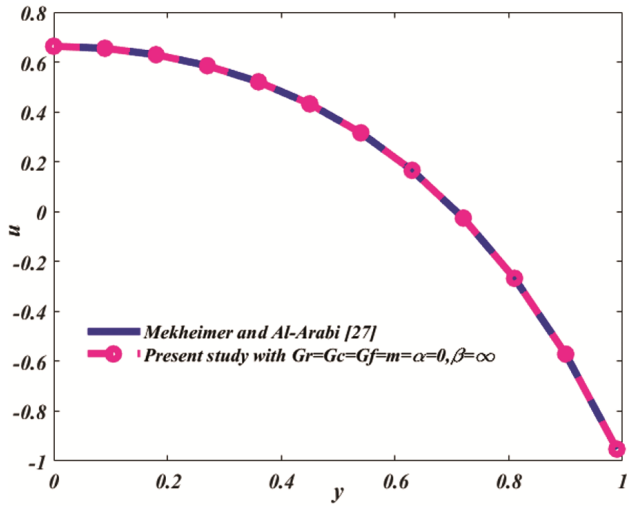

Fig. 10 — Validation of the present study with the reported literature

increase, it is evident that the Nusselt number also increases. Nevertheless, the radiation parameter exhibits the opposite tendency. It is evident that the Sherwood number decreases with increasing P_r, N_b, N_t, Q, whereas the Sherwood number increases with increasing radiation parameter R_d.

Validation of the Results

For validation, we compared the profile of the fluid velocity with that reported by Mekheimer and Al-Arabi[27]. Hereby fixing $G_r = G_c = G_f = m = \alpha = 0 \; and \; \beta = \infty$, the velocity profile of the present investigation has coincided with Mekheimer and Al-Arabi[27] (Fig. 10).

Conclusion

The integration of double diffusive convection, peristaltic transport, magnetohydrodynamics (MHD), porous media, and thermal radiation within a symmetric channel provides a detailed framework for analysing complex transport phenomena in both natural and engineered systems. The interactions play a critical role in determining flow stability, heat and mass transfer rates, as well as the overall efficiency across a range of applications. Such studies are essential in the field of biomedical engineering for modelling blood flow in arteries when subjected to magnetic fields. Solving the non-linear differential equations was done using the homotopy perturbation approach. Through the use of graphical findings, the impacts of the different physical properties of the flow amounts were also seen. An overview of some of the fascinating findings from the present study is provided below:

- The temperature profile grew in tandem with increases in the values of the heat source/sink parameter, Dufour number, thermophoresis parameter, and Brownian motion parameter. On the other hand, the pattern is reversed when considering the radiation parameter.
- The concentration profile is improved by increasing the radiation parameter values; nevertheless, the thermophoresis number, Soret parameter, and Brownian motion parameter showed a trend in the opposite direction.
- In contrast to the nanoparticle fraction, which fell as the thermophoresis parameter grew, the nanoparticle fraction increased as the Brownian motion parameter increased.
- As the radiation, Darcy number, and magnetic parameters grew, so did the size of the trapped masses.

Conflict of interest

The authors declare no conflict of interest.

Supplementary Information

Supplementary information is available on the website https://nopr.niscpr.res.in/handle/123456789.

References

1 Latham W, Fluid motions in a peristaltic pump, Doctoral dissertation (Massachusetts Institute of Technology, (1966).
2 Fung Y C & Yih C S, *Peristaltic transport*, (1968).
3 Shapiro A H, Jaffrin M Y & Weinberg S L, Peristaltic pumping with long wavelengths at low Reynolds number, *J Fluid Mech*, 37 (1969) 799.
4 Alokaily S, Feigl K & Tanner F X, Characterization of peristaltic flow during the mixing process in a model human stomach, *Phys Fluids*, 31 (2019) 103105.
5 Shahmir N, Ramzan M, Akram J, Kadry S, Alshahrani S & Li S, Peristaltic flow of ethylene glycol and water mixture-based hybrid nanofluid in an asymmetric channel, *Bio-Nano Sci*, 14 (2023) 517.
6 Mishra M & Rao A R, Peristaltic transport of a Newtonian fluid in an asymmetric channel, *Zeitschrift Für Angewandte Mathematik Und Physik*, 54 (2003) 532.
7 Srinivas A N S, Haseena C & Sreenadh S, Peristaltic transport of nanofluid in a vertical porous stratum with heat transfer effects, *Bio-Nano Sci*, 9 (2019) 117.
8 Sucharitha G, Lakshminarayana P & Sandeep N, MHD and cross diffusion effects on peristaltic flow of a Casson nanofluid in a duct, *Appl Math Sci Comput*, 2 (2019) 191.
9 Thirunavukarasan K & Sucharitha G, Thermal performance and MHD peristaltic flow of hybrid nanofluid (Au-Ta/Blood) in an asymmetric conduit with electro-osmosis and shape factor effects, *Case Stud Therm Eng*, 66 (2025) 105708.
10 Ramakrishnan G, Bandi R, Seelam R & Pallavarapu L, Influence of slip boundary conditions on Jeffrey fluid flow in tapered conduit with hall current and Soret-Dufour effects, *Chem Eng Technol*, 47 (2024) 1082.

11 Rani P N & Sarojamma G, Peristaltic transport of a Casson fluid in an asymmetric channel, *Aust Phys Eng Sci Med*, 27 (2004) 49.

12 Nagarani P, Peristaltic transport of a Casson fluid in an inclined channel, *Korea Aust Rheol J*, 22 (2010) 105.

13 Pandey S K & Tripathi D, Peristaltic transport of a Casson fluid in a finite channel: application to flows of concentrated fluids in oesophagus, *Int J Biomath*, 3 (2010) 453.

14 Gudekote M & Choudhari R, Slip effects on peristaltic transport of Casson fluid in an inclined elastic tube with porous walls, *J Adv Res Fluid Mech Therm Sci*, 43 (2018) 67.

15 Rajashekhar C, Manjunatha G, Vaidya H, Divya B & Prasad K, 2018. Peristaltic flow of Casson liquid in an inclined porous tube with convective boundary conditions and variable liquid properties, *Front Heat Mass Transf*, 11 (2018) 1

16 Devaki P, Sreenadh S, Vajravelu K, Prasad K V & Vaidya H, Wall properties and slip consequences on peristaltic transport of a Casson liquid in a flexible channel with heat transfer, *Appl Math Nonlin Sci*, 3 (2018) 277.

17 Hasan M M, Samad M A & Hossain M M, Peristaltic transport of casson fluid in a porous channel in presence of hall current, *Appl Internet Things*, (2021) 27.

18 Choi S U & Eastman J A, Enhancing thermal conductivity of fluids with nanoparticles (No. ANL/MSD/CP-84938; CONF-951135-29). Argonne National Lab.(ANL), Argonne, IL (United States), (1995).

19 Mustafa M, Hina S, Hayat T & Alsaedi A, Influence of wall properties on the peristaltic flow of a nanofluid: analytic and numerical solutions, *Int J Heat Mass Transf*, 55 (2012) 4871.

20 Abbasi F M, Hayat T & Ahmad B, Peristaltic transport of copper-water nanofluid saturating porous medium, *Physica E: Low-Dimens Syst Nanostruct*, 67 (2015) 47.

21 Akbar N S, Nadeem S, Hayat T & Hendi A A, Peristaltic flow of a nanofluid in a non-uniform tube, *Heat Mass Transfer*, 48 (2012) 451.

22 Ajithkumar M, Lakshminarayana P & Vajravelu K, Diffusion effects on mixed convective peristaltic flow of a bi-viscous Bingham nanofluid through a porous medium with convective boundary conditions, *Phys Fluids*, 35 (2023) 032008.

23 Nadeem S, Mushtaq A, Alzabut J, Ghazwani H A & Eldin S M, The flow of an Eyring Powell Nanofluid in a porous peristaltic channel through a porous medium, *Sci Rep*, 13 (2023) 9694.

24 Reddappa B & Geetha R, Effects of second order chemical reaction on MHD forced convection Cu, Ag, and Fe_3O_4 nanoparticles of Jeffrey Nanofluid over a moving plate in a porous medium in the presence of heat source/sink, *J Integr Sci Technol*, 12 (2024) 762.

25 Geetha R, Reddappa B, Tarakaramu N, Kumar B R & Khan I M, Effect of double stratification on MHD Williamson boundary layer flow and heat transfer across a shrinking/stretching sheet immersed in a porous medium, *Int J Chem Eng*, 2024 (2024) 9983489.

26 Ajithkumar M & Lakshminarayana P, MHD peristaltic flow of chemically reactive Casson nanofluid in a nonuniform porous inclined flexible channel with cross-diffusion effects, *Int J Mod Phys B*, 37 (2023) 2350292.

27 Mekheimer K S & Al-Arabi T H, Nonlinear peristaltic transport of MHD flow through a porous medium. *International Journal of Mathematics and Mathematical Sciences*, 26 (2003) 1663.

28 Akram S, Athar M, Saeed K & Razia A, Influence of an induced magnetic field on double diffusion convection for peristaltic flow of thermally radiative Prandtl nanofluid in non-uniform channel, *Tribol Int*, 187 (2023) 108719.

29 Eldabe N T, Abouzeid M & Shawky H A, MHD peristaltic transport of Bingham blood fluid with heat and mass transfer through a non-uniform channel, *J Adv Res Fluid Mech Therm Sci*, 77 (2021) 145.

30 Abd-Alla A M, Abo-Dahab S M, Thabet E N & Abdelhafez M A, Impact of inclined magnetic field on peristaltic flow of blood fluid in an inclined asymmetric channel in the presence of heat and mass transfer, *Waves Random Complex Media*, 35 (2022) 7142.

31 Abbasi A, Khan S U, Farooq W, Mughal F M, Khan M I, Prasannakumara B C, El-Wakad M T, Guedri K & Galal A M, Peristaltic flow of chemically reactive Ellis fluid through an asymmetric channel: Heat and mass transfer analysis, *Ain Shams Eng J*, 14 (2023) 101832.

32 Iqbal J, Abbasi F M, Alkinidri M & Alahmadi H, Heat and mass transfer analysis for MHD bioconvection peristaltic motion of Powell-Eyring nanofluid with variable thermal characteristics, *Case Stud Therm Eng*, 43 (2023) 102692.

33 Ravikumar S, Khan M I, Al-Qahtani S A & Eldin S M, Significance of heat and mass transport in peristaltic flow of Jeffrey material subject to chemical reaction and radiation phenomenon through a tapered channel, *Open Phys*, 21 (2023) 20220258.

34 Noreen S & Waheed S, Study of heat characteristics of electroosmotic mediator and peristaltic mechanism via porous microtube, *Bio-Nano Sci*, 11 (2021) 476.

35 Iqbal J, Abbasi F M & Nawaz R, Study of mass and heat transfer for peristaltic transport of cross nanofluid through a curved channel, *J Applied Mathematics and Mechanics/ Zeitschrift für AngewandteMathematik und Mechanik*, 104 (2024) 1.

36 Das S & Barman B, Ramification of hall and ion-slip currents on electro-osmosis of ionic hybrid nanofluid in a peristaltic microchannel, *Bio-Nano Sci*, 12 (2022) 957.

37 Gudekote M, Choudhari R, Sanil P, Hadimani B, Vaidya H & Prasad K V, 2024. MHD effects on the peristaltic transport of non-newtonian eyring-powell fluid with heat and mass transfer in an inclined uniform channel, *Arabian Journal for Science and Engineering*, 49 (2024) 15143.

38 Reddappa B, Parandhama A & Sreenadh S, Peristaltic transport of conducting Williamson fluid in a porous channel, *J Math Comput Sci*, 10 (2019) 277.

39 Gangavathi P, Jyothi S, Reddy M S & Reddy P Y, Slip and hall effects on the peristaltic flow of a Jeffrey fluid through a porous medium in an inclined channel, *Mater Today: Proc*, 80 (2023) 1970.

40 Jawad Q K & Abdulhadi A M, Influence of MHD and porous media on peristaltic transport for nanofluids in an asymmetric channel for different types of walls, *Int J Nonl Anal Appl*, 14 (2023) 819.

41 Moatimid G M, Mohamed M A & Elagamy K, Microorganisms'peristaltic transport within a carreau nanofluid through a modified darcy porous medium, *Special Top Rev Porous Media: An Int J*, 14 (2023) 1.

42 Akram S, Saeed K, Athar M, Razia A, Hussain A & Naz I, Convection theory on thermally radiative peristaltic flow of Prandtl tilted magneto nanofluid in an asymmetric channel

with effects of partial slip and viscous dissipation, *Mater Today Commun*, 35 (2023) 106171.

43 Khan Y, Akram S, Razia A, Hussain A & Alsulaimani H A, Effects of double diffusive convection and inclined magnetic field on the peristaltic flow of fourth grade nanofluids in a non-uniform channel, *Nanomaterials*, 12 (2022) 3037.

44 Ganesan S & Vasanthakumari R, Influence of magnetic field and thermal radiation on peristaltic motion with double-diffusive convection in Jeffery nanofluids, *Heat Transf*, 49 (2020) 2025.

45 Saeed K, Akram S, Ahmad A, Athar M, Imran M & Muhammad T, Impact of partial slip on double diffusion convection and inclined magnetic field on peristaltic wave of six-constant Jeffreys nanofluid along asymmetric channel, *Eur Phys J Plus*, 137 (2022) 364.

46 Khan Y, Athar M, Akram S, Saeed K, Razia A & Alameer A, Roll of partial slip on Ellis nanofluid in the proximity of double diffusion convection and tilted magnetic field: Application of Chyme movement, *Heliyon*, 9 (2023) e14760.

47 Akram S, Athar M, Saeed K & Razia A, Theoretical analysis of partial slip on double-diffusion convection of Eyring-Powell nanofluids under the effects of peristaltic propulsion and inclined magnetic field, *J Magn Magn Mater*, 569 (2023) 170445.

48 Athar M, Khan Y, Akram S, Saeed K, Alameer A & Hussain A, Consequence of double-diffusion convection and partial slip on magneto-oldroyd-4 constants nanofluids with peristaltic propulsion in an asymmetric channel, *Complexity*, 2022 (2022) 7634357.

49 Khan Y, Akram S, Athar M, Saeed K, Muhammad T, Hussain A, Imran M & Alsulaimani H A, The role of double-diffusion convection and induced magnetic field on peristaltic pumping of a Johnson–Segalman nanofluid in a non-uniform channel, *Nanomaterials*, 12 (2022) 1051.

50 Ajithkumar M, Lakshminarayana P & Vajravelu K, Peristaltic flow of bioconvective Ree–Eyring nanofluid through an inclined elastic channel with partial slip effects, *J Appl Phys*, 134 (2023) 154701.

51 Abou-Zeid M, Effects of thermal-diffusion and viscous dissipation on peristaltic flow of micropolar non-Newtonian nanofluid: Application of homotopy perturbation method, *Results Phys*, 6 (2016) 481.

52 Ajithkumar M & Lakshminarayana P, Chemically reactive MHD peristaltic flow of Jeffrey nanofluid via a vertical porous conduit with complaint walls under the effects of bioconvection and double diffusion, *Int J Mod Phys B*, 38 (2023) 2450203.

53 Sucharitha G, Vajravelu K & Lakshminarayana P, Effect of heat and mass transfer on the peristaltic flow of a Jeffrey nanofluid in a tapered flexible channel in the presence of aligned magnetic field, *Eur Phys J Special Top*, 228 (2019) 2713.